International Journal for Modern Trends in Science and Technology
Volume 12, Issue 04, pages 670-683.
ISSN: 2455-3778 online
Available online at: http://www.ijmtst.com/vol12issue04.html
DOI: https://doi.org/10.5281/zenodo.19536627

Bidirectional EV Onboard Charging Using a Power-Quality-Optimized Interleaved Totem-Pole and Push–Pull Converter for V2G Applications

J. Anand, M. Durga Prasad, N. Akhil Vishal, M. Lavanya, Mandala Pujitha

Department of Electrical and Electronics Engineering, Vasireddy Venkatadri Institute of Technology, Pedakakani, Namburu, Guntur, India.

To Cite this Article
J. Anand, M. Durga Prasad, N. Akhil Vishal, M. Lavanya & Mandala Pujitha (2026). Bidirectional EV Onboard Charging Using a Power-Quality-Optimized Interleaved Totem-Pole and Push–Pull Converter for V2G Applications. International Journal for Modern Trends in Science and Technology, 12(04), 670-683. https://doi.org/10.5281/zenodo.19536627

Article Info
Received: 16 March 2026; Revised: 06 April 2026; Accepted: 10 April 2026.

KEYWORDS

Bidirectional Onboard Charger, Interleaved Totem-Pole Converter, Push–Pull Converter, Power Quality Improvement, Vehicle-to-Grid (V2G), Electric Vehicle Charging, Power Factor Correction.

ABSTRACT

This paper proposes a power-quality-enhanced bidirectional interleaved totem-pole converter–based onboard charger (OBC) for electric vehicle (EV) applications, aimed at reducing power conversion stages, improving efficiency, and enabling vehicle-to-grid (V2G) operation. Conventional two-stage OBC architectures employ a diode bridge rectifier (DBR) followed by a front-end boost converter for power factor correction (PFC) and a back-end isolated push–pull converter for battery charging. Although effective, these structures suffer from increased conduction losses, higher component count, reduced power density, and inherently unidirectional power flow, limiting operation to grid-to-vehicle (G2V) mode. To address these limitations, the proposed system replaces the DBR, boost PFC, and push–pull stages with a bidirectional interleaved totem-pole AC–DC converter utilizing fully active switches. In conventional push–pull converters, passive diode rectifiers on the transformer secondary side restrict power flow to unidirectional operation. In contrast, the proposed topology employs actively controlled switches on both sides of the converter, enabling controlled bidirectional energy transfer between the grid and the EV battery. The proposed configuration significantly reduces component count, eliminates diode conduction losses, and achieves near-unity power factor with low input current harmonic distortion. The interleaved structure effectively minimizes current ripple, improves thermal distribution, and enhances power density. An advanced control strategy is implemented to regulate the dc-bus voltage, ensure constant-current/constant-voltage (CC/CV) battery charging, and maintain high power quality under varying grid and load conditions. Simulation results

verify that the proposed OBC delivers superior power factor, reduced switching and conduction losses, improved efficiency, and reliable bidirectional G2V/V2G operation compared to conventional unidirectional OBC architectures, making it a promising solution for next-generation EV charging and grid-interactive applications.

1. INTRODUCTION

The increasing adoption of electric vehicles in modern transportation systems has significantly influenced the development of advanced power electronic converters for efficient energy conversion and management. Onboard chargers play a vital role in electric vehicles by facilitating the transfer of electrical energy from the grid to the vehicle battery. Conventional onboard charger architectures typically employ a two stage configuration consisting of a diode bridge rectifier followed by a boost type power factor correction converter and an isolated dc dc converter for battery charging. Although this approach is widely adopted due to its simplicity and reliability, it suffers from several inherent limitations such as increased conduction losses, bulky passive components, higher component count, and reduced overall efficiency [1]. Moreover, the presence of passive diode rectifiers restricts the power flow to unidirectional operation, thereby limiting the system to grid to vehicle mode only and preventing the realization of vehicle to grid functionality [2]. With the growing need for sustainable energy systems and smart grid integration, electric vehicles are increasingly being viewed as distributed energy storage units capable of interacting with the grid. Vehicle to grid technology enables bidirectional power flow between the vehicle battery and the grid, allowing electric vehicles to support grid operations such as peak load shaving, frequency regulation, and voltage stabilization [3]. This paradigm shift necessitates the development of bidirectional onboard chargers that can efficiently operate in both charging and discharging modes while maintaining high power quality and system reliability. Conventional unidirectional charger topologies are not suitable for such applications due to their limited functionality and inefficiency in handling reverse power flow [4]. In recent years, significant research efforts have been directed towards improving the efficiency and performance of ac dc conversion stages used in onboard chargers. The totem pole converter has emerged as a promising topology due to its ability to eliminate the diode bridge rectifier and utilize actively controlled switches for rectification. This results in reduced conduction losses and improved efficiency, particularly at high power levels [5]. The use of wide bandgap semiconductor devices such as silicon carbide and gallium nitride further enhances the performance of totem pole converters by enabling high frequency switching, reduced switching losses, and improved thermal characteristics [6]. Despite these advantages, single phase totem pole converters often experience issues related to current ripple, electromagnetic interference, and uneven thermal distribution, which can affect system performance and reliability [7]. To overcome these challenges, interleaving techniques have been widely adopted in power converter design. Interleaved converters consist of multiple parallel phases that operate with phase shifted switching signals, resulting in reduced input and output current ripple, improved efficiency, and better thermal management [8]. The interleaving approach also allows for smaller passive components and increased power density, making it highly suitable for onboard charger applications where size and weight are critical considerations [9]. By combining the advantages of totem pole topology and interleaving, it is possible to achieve a highly efficient and compact ac dc conversion stage with superior power quality performance [10]. The isolated dc dc conversion stage is another important component of onboard chargers, as it provides galvanic isolation and regulates the battery charging process. Among various isolated converter topologies, the push pull converter is widely used due to its simple structure, efficient utilization of the transformer, and suitability for medium power applications [11]. However, in conventional designs, the use of diode rectifiers on the secondary side limits the converter to unidirectional operation. This restricts the ability of the system to support bidirectional energy transfer, which is essential for vehicle to grid applications [12]. By replacing passive rectifiers with actively controlled switches, the push pull converter can be modified to support bidirectional operation, enabling controlled energy flow between the

grid and the vehicle battery [13]. Power quality is a critical aspect of onboard charger design, as poor power factor and high harmonic distortion can negatively impact the grid and violate regulatory standards such as IEEE 519. High quality power conversion requires the input current to be sinusoidal and in phase with the grid voltage, thereby achieving near unity power factor and low total harmonic distortion [14]. Advanced control strategies are essential to achieve these objectives while ensuring stable operation under varying grid and load conditions. Techniques such as proportional integral control, predictive control, and adaptive control have been extensively studied for improving the dynamic response and robustness of power converters [15]. In addition, the coordination between the ac dc and dc dc stages plays a crucial role in maintaining dc bus voltage stability and ensuring efficient battery charging under constant current and constant voltage modes [16]. The integration of bidirectional onboard chargers with smart grid infrastructure further enhances the capabilities of electric vehicles by enabling them to participate in grid support services. Electric vehicles can act as mobile energy storage units that can absorb excess energy during off peak periods and supply energy back to the grid during peak demand [17]. This not only improves grid stability but also enhances the utilization of renewable energy sources such as solar and wind power. Several studies have demonstrated the potential of vehicle to grid technology in reducing energy costs, improving grid reliability, and supporting renewable energy integration [18]. However, achieving efficient and reliable V2G operation requires advanced converter topologies that can handle bidirectional power flow with minimal losses and high power quality [19]. In this context, this paper proposes a power quality optimized bidirectional interleaved totem pole and push pull converter for electric vehicle onboard charging applications. The proposed topology eliminates the need for a diode bridge rectifier and multiple conversion stages, thereby reducing losses and improving efficiency. The use of interleaving minimizes current ripple and enhances thermal performance, while the implementation of actively controlled switches in both ac dc and dc dc stages enables seamless bidirectional power flow [20]. An advanced control strategy is employed to regulate the dc bus voltage, maintain near unity power factor, and ensure proper battery charging under constant current and constant voltage modes. The effectiveness of the proposed system is validated through simulation results, which demonstrate improved efficiency, reduced harmonic distortion, and reliable operation in both grid to vehicle and vehicle to grid modes.

II. SYSTEM CONFIGURATION

The proposed system consists of a bidirectional onboard charger (OBC) integrating an AC–DC totem-pole converter, a solar PV-based DC–DC boost converter, and an isolated push–pull DC–DC converter for EV battery interfacing. The configuration is designed to support bidirectional power flow for both grid-to-vehicle (G2V) and vehicle-to-grid (V2G) operations while improving efficiency and power quality. On the grid side, an AC–DC totem-pole voltage source converter (VSC) using switches S1–S4 and input inductor Lf is employed. This converter performs power factor correction by ensuring the grid current (Is) is sinusoidal and in phase with the grid voltage. It also regulates the DC-link voltage (Vdc) across capacitor Cdc, eliminating the need for a diode bridge and reducing conduction losses. A solar PV system is connected through a DC–DC boost converter, which includes an inductor, switch, diode, and capacitor. This stage boosts the PV voltage (Vpv) and transfers power to the DC-link, enabling renewable energy integration and supporting the load demand. The DC-link feeds an isolated push–pull converter consisting of high-frequency transformers and switches G1–G4. Unlike conventional designs, active switches are used on both primary and secondary sides, enabling bidirectional energy transfer between the DC-link and the EV battery. This allows both charging and discharging operations. At the output, an LC filter (Ls and Cs) smooths the voltage and current supplied to the EV battery, ensuring stable operation. The battery voltage (Vev) and current (Iev) are controlled for proper charging and discharging. Overall, the system integrates grid, PV, and EV through a common DC-link, enabling efficient energy management, reduced losses, and reliable bidirectional operation suitable for modern EV and smart grid applications.

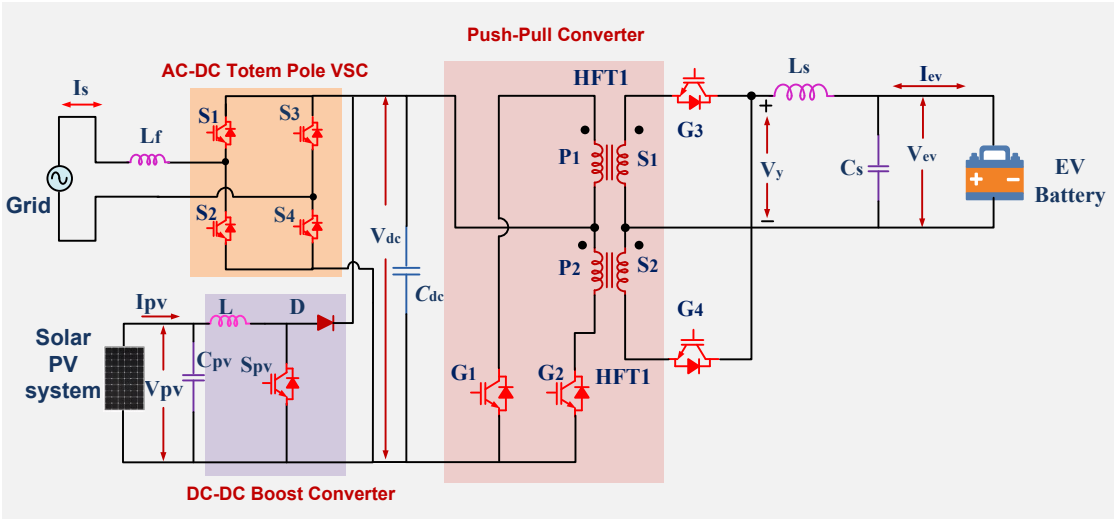

Fig. 1. Proposed Bidirectional OBC with Solar PV and EV Battery Integration

III. MODELING AND DESIGN OF PROPOSED SYSTEM CONFIGURATION

A. Single-Diode Solar PV System

The solar photovoltaic system is commonly modeled using the single-diode equivalent circuit, which provides an accurate representation of PV characteristics under varying environmental conditions. In this model, the PV cell consists of a current source representing the photo-generated current, a diode, and series and shunt resistances accounting for internal losses. The output current of the PV system is expressed as

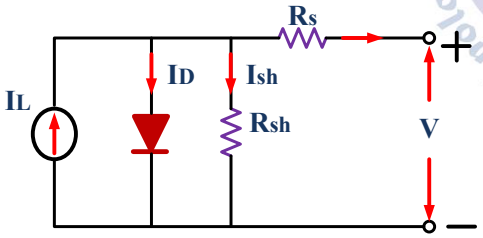

Fig. 2 equivalent model of PV solar.

$$I_{pv} = I_{ph} - I_o\left[\exp\left(\frac{V_{pv} + I_{pv}R_s}{aV_t}\right) - 1\right] - \frac{V_{pv} + I_{pv}R_s}{R_{sh}} \quad (1)$$

The generated photocurrent depends on solar irradiance and temperature, and is given by

$$I_{ph} = [I_{sc,ref} + K_i(T - T_{ref})]\frac{G}{G_{ref}} \quad (2)$$

The output power of the PV system is

$$P_{pv} = V_{pv}I_{pv} \quad (3)$$

The power-voltage characteristic of the PV panel exhibits a unique maximum power point (MPP) at which the power is maximum. This condition is defined by

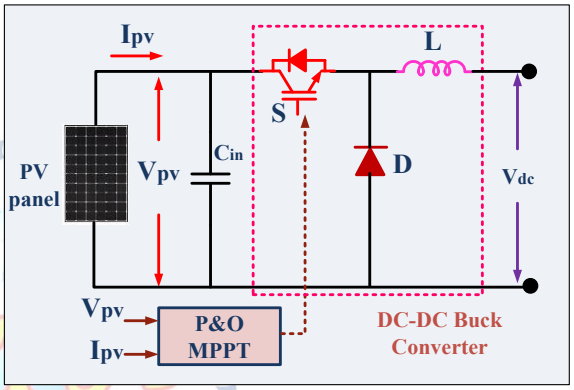

Fig. 3 solar PV P&O MPPT DC-DC Buck converter

$$\frac{dP}{dV} = 0 \quad (4)$$

To ensure that the PV system always operates at this maximum power point, a boost converter is used along with a maximum power point tracking (MPPT) algorithm. The boost converter steps up the PV voltage and adjusts the operating point by controlling the duty cycle. The voltage gain of the boost converter is given by

$$V_o = \frac{V_{pv}}{1 - D} \quad (5)$$

where D is the duty ratio. By varying D, the input voltage and current of the PV system are controlled.

The inductor and capacitor of the boost converter are designed based on ripple considerations. The inductance is given by

$$L = \frac{V_{pv}D}{\Delta I_L f_s} \quad (6)$$

and the output capacitor is selected as

$$C = \frac{I_o D}{\Delta V_o f_s} \quad (7)$$

B. P&O MPPT Boost Converter

The Perturb and Observe (P&O) MPPT algorithm is used to track the maximum power point. In this method, the PV voltage or duty cycle is slightly perturbed and the resulting change in power is observed. The power is calculated as

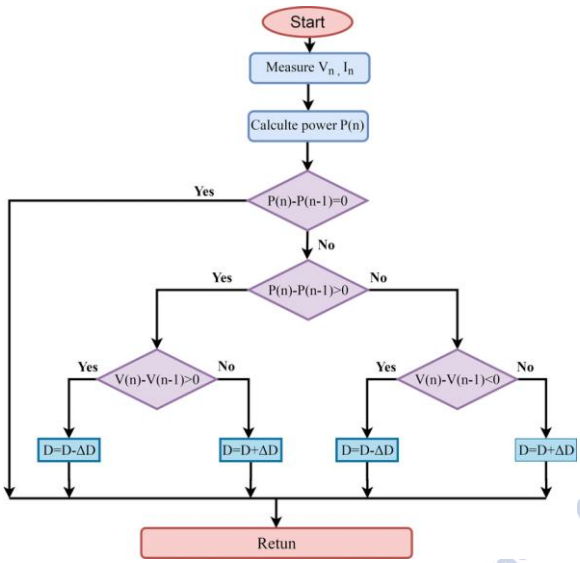

Fig.4 flow chart of P&O MPPT algorithm

$$P(k) = V(k)I(k) \tag{7}$$

The changes in power and voltage are given by

$$\Delta P = P(k) - P(k-1) \tag{8}$$

$$\Delta V = V(k) - V(k-1) \tag{9}$$

Based on these values, the duty cycle is updated as

$$D(k) = D(k-1) \pm \Delta D \tag{10}$$

If the power increases after perturbation, the operating point moves toward the maximum power point and the perturbation continues in the same direction. If the power decreases, the direction is reversed. Overall, the combination of the single-diode PV model, boost converter, and P&O MPPT algorithm ensures efficient extraction of maximum power from the PV system under varying irradiance and temperature conditions. The boost converter provides voltage regulation, while the MPPT algorithm continuously adjusts the operating point to achieve optimal performance.

IV. Isolated converter DC-DC Converters

A Bidirectional Isolated DC–DC Push–Pull Converter

A bidirectional isolated DC–DC push–pull converter is a widely used topology in electric vehicle (EV) onboard chargers and energy storage systems where efficient and controlled power transfer between two DC sources is required. Unlike conventional converters, which allow only unidirectional power flow, bidirectional converters enable energy transfer in both directions, supporting both grid-to-vehicle (G2V) and vehicle-to-grid (V2G) operations. The push–pull converter is an isolated topology that employs a center-tapped transformer, providing galvanic isolation, voltage matching, and improved safety.

In conventional push–pull converters, diode rectifiers are used on the secondary side, restricting the direction of power flow. However, in a bidirectional configuration, these diodes are replaced with actively controlled switches, allowing reversible energy transfer. The use of active switches reduces conduction losses and enhances efficiency. The performance of the converter is governed by switching frequency, duty cycle, transformer turns ratio, and load conditions.

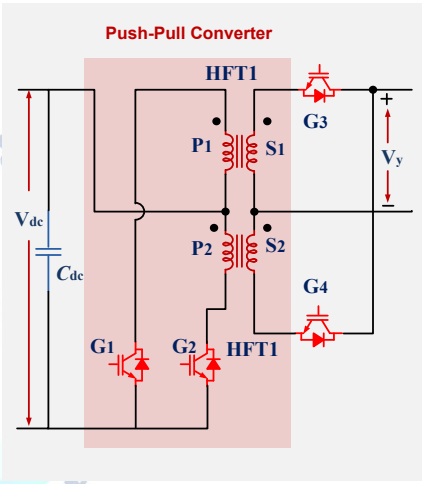

Fig. 5 Basic Push-Pull Converters

B. Working Principle with Fundamental Equations

The operation of the push–pull converter is based on alternate switching of two power switches connected to a center-tapped primary winding of a transformer. Each switch conducts for a duration defined by the duty cycle D, producing an alternating voltage across the transformer.

The instantaneous primary voltage is:

$$V_p(t) = V_{in} \tag{11}$$

The secondary voltage induced in the transformer is:

$$V_s(t) = \frac{N_s}{N_p} \cdot V_{in} \tag{12}$$

After rectification and filtering, the average output voltage becomes:

$$V_o = 2 \cdot D \cdot \frac{N_s}{N_p} \cdot V_{in} \tag{13}$$

This factor of 2 appears because both halves of the transformer contribute during one switching cycle.

The output current is given by:

$$I_o = \frac{P_o}{V_o} \quad (14)$$

and input power is:

$$P_{in} = V_{in} \cdot I_{in} \quad (15)$$

Considering efficiency η:

$$\eta = \frac{P_o}{P_{in}} \quad (16)$$

Inductor and Ripple Equations

The output inductor smooths the current and its value is determined by allowable ripple:

$$L = \frac{V_L \cdot D}{\Delta I_L \cdot f_s} \quad (17)$$

where:

VL=Vs−Vo

ΔIL= inductor ripple current

fs = switching frequency

The ripple current is:

$$\Delta I_L = \frac{(V_s - V_o) \cdot D}{L \cdot f_s} \quad (18)$$

Output voltage ripple is:

$$\Delta V_o = \frac{I_o \cdot D}{C \cdot f_s} \quad (19)$$

C. Operation of the Converter

The converter operates by alternately switching the primary-side switches S1S_1S1 and S2S_2S2, creating a high-frequency AC voltage across the transformer. During each switching interval, only one switch conducts, ensuring that current flows through one half of the primary winding at a time. This alternating excitation prevents transformer core saturation and allows efficient energy transfer.

On the secondary side, active switches replace diodes, enabling synchronous rectification during forward operation and inversion during reverse operation. The converter can operate in continuous conduction mode (CCM), where the inductor current never falls to zero, ensuring smooth current flow and reduced losses.

The magnetizing current of the transformer is:

$$I_m = \frac{V_{in} \cdot D}{L_m \cdot f_s} \quad (20)$$

Where Lm is the magnetizing inductance.

D. Modes of Operation

a. Forward Mode (G2V Operation)

In forward mode, energy flows from the input DC source (grid/DC link) to the battery.

During Interval 1, switch S1 is ON:

- Primary voltage = Vin
- Secondary voltage = Ns/ Np*Vin
- Energy is transferred to the output

During **Interval 2**, switch S2 is ON:

- Current flows through the other half of the transformer
- Continuous energy transfer is maintained

The average output voltage is:

$$V_o = 2D \cdot \frac{N_s}{N_p} \cdot V_{in} \quad (21)$$

The duty cycle is limited to:

$$D \leq 0.5 \quad (22)$$

to avoid transformer saturation.

b. Reverse Mode (V2G Operation)

In reverse mode, power flows from the battery to the grid/DC link.

Now the secondary side switches generate AC, and the transformer transfers energy to the primary side.

The voltage relationship becomes:

$$V_{in} = 2D \cdot \frac{N_p}{N_s} \cdot V_o \quad (23)$$

The current direction reverses, and power delivered is:

$$P = V_o \cdot I_o = V_{in} \cdot I_{in} \quad (24)$$

In this mode, the converter behaves like an inverter followed by a rectifier.

c. Switch Stress and Transformer Considerations

The voltage stress on each switch is:

$$V_{switch} = 2 \cdot V_{in} \quad (25)$$

Peak current through switches:

$$I_{peak} = I_o \cdot \frac{N_p}{N_s} \quad (26)$$

Transformer design must satisfy:

$$B_{max} = \frac{V_{in} \cdot D}{N_p \cdot A_e \cdot f_s} \quad (27)$$

where: Bmax = maximum flux density, A = core cross-sectional area

V. Modeling and Designing of Lithium-Ion Battery.

In modern power systems, Hybrid Energy Storage Systems (HESS) integrates multiple energy storage devices to enhance overall energy and power performance. Lithium-ion batteries, owing to their high energy density and efficiency, are widely utilized for sustained energy supply in such systems. The incorporation of multiple battery units facilitates improved operational flexibility and effective load management under varying conditions. This configuration enables enhanced load balancing, mitigates stress on individual battery units, and extends overall battery lifespan. Furthermore, it improves system responsiveness and reliability, making it highly suitable for applications such as electric vehicle (EV) charging, renewable energy integration, and microgrid operations.

a. Lithium-Ion Battery Modeling

The lithium-ion battery used in the proposed system is modeled using a nonlinear dynamic equation that captures both charging and discharging characteristics. The battery terminal voltage is expressed as:

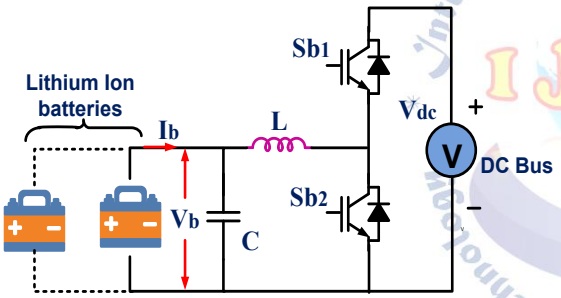

Fig.6 principle operation bidirectional dc-dc buck boost converter

$$E_B = E_0 - \frac{KQI_B}{Q - \int I_B\,dt} - k\frac{Q}{Q - \int I_B\,dt}\int I_B dt + A\exp(-B\int I_B\,dt) \quad (28)$$

where E_B represents the battery terminal voltage, E_0 is the constant open-circuit voltage, K denotes the polarization constant (V/Ah), Q is the maximum battery capacity (Ah), and IB is the battery current. The term $\int I_B\,dt)$ represents the extracted capacity over time. The exponential term $\exp(-B\int I_B\,dt)$ models the voltage behavior in the exponential region of the battery discharge curve, where A and B are empirical constants. This model effectively captures the nonlinear voltage characteristics of lithium-ion batteries under varying load conditions. It accounts for polarization effects, capacity variation, and transient response during charging and discharging. The State of Charge (SoC) of the battery is estimated based on the integration of battery current, enabling accurate monitoring and control of energy storage units. The developed battery model is implemented for each BESS unit in the system, allowing decentralized control and SoC balancing across multiple batteries to enhance system reliability and lifespan.

VI. WORKING AND OPERATION OF TOTEM-POLE PFC CONVERTER AND PV BOOST CONVERTER

The totem-pole power factor correction converter and the PV boost converter are connected across the common DC-link capacitor, while the EV-side converter and battery are considered as an equivalent load. The main objective of this stage is to regulate the DC-link voltage, shape the grid current into a sinusoidal waveform with low harmonic distortion, and simultaneously transfer the PV power to the DC link. During the positive half cycle of the grid voltage, switch S4 remains ON and switch S3 remains OFF. During the negative half cycle, switch S3 remains ON and switch S4 remains OFF. In both half cycles, switches S1, S2, and Spv are controlled according to the duty ratios of the PFC stage and PV boost stage.

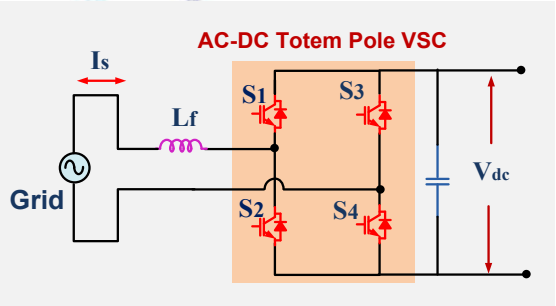

Fig. 7. Operation of Totem-Pole PFC Converter and PV Boost Converter

The grid-side inductor voltage is governed by

$$v_{L_f} = L_f\frac{di_s}{dt} \quad (29)$$

where Lf is the input inductor and is is the grid current. The PV-side boost inductor voltage is

$$v_{L_{pv}} = L_{pv}\frac{di_{pv}}{dt} \quad (30)$$

where Lpv is the PV boost inductor and ipv is the PV current. The DC-link capacitor dynamics can be written as

$$C_{dc}\frac{dV_{dc}}{dt} = i_{dc,in} - i_{dc,out} \quad (31)$$

where Vdc is the DC-link voltage, idc,in is the current supplied by the grid and PV stages, and idc,out is the current drawn by the EV-side converter.

During the positive half cycle, the operation can be explained using the three switching states given in Table II.

In State 1, switches S2, S4, and Spv are ON, while S1 and S3 are OFF. In this condition, the grid-side inductor Lf is energized through the path formed by the source and active switches, and the PV inductor Lpv is also energized because Spv is ON. Hence, the inductor voltages are

$$v_{L_f} = v_s \tag{32}$$

$$v_{L_{pv}} = V_{pv} \tag{33}$$

Thus, both inductors store energy and their currents increase linearly as

$$\frac{di_s}{dt} = \frac{v_s}{L_f} \tag{34}$$

$$\frac{di_{pv}}{dt} = \frac{V_{pv}}{L_{pv}} \tag{35}$$

where vs is the instantaneous grid voltage and Vpv is the PV voltage.

In **State 2**, switches S1, S4, and Spv are ON, while S2 and S3 are OFF. In this state, the grid-side inductor releases energy to the DC-link capacitor and load, while the PV inductor continues charging because Spv is still ON. Therefore, the inductor voltages become

$$v_{L_f} = v_s - V_{dc} \tag{36}$$

$$v_{L_{pv}} = V_{pv} \tag{37}$$

and the current slopes are

$$\frac{di_s}{dt} = \frac{v_s - V_{dc}}{L_f} \tag{38}$$

$$\frac{di_{pv}}{dt} = \frac{V_{pv}}{L_{pv}} \tag{39}$$

Since generally Vdc>vs, the grid inductor current decreases in this interval, transferring stored energy to the DC-link.

In **State 3**, switches S1 and S4 are ON, Spv is OFF, and S2 , S3 are OFF. In this condition, the grid-side inductor continues to transfer energy to the DC link, while the PV boost inductor releases its stored energy through the diode to the DC-link capacitor. Hence,

$$v_{L_f} = v_s - V_{dc} \tag{40}$$

$$v_{L_{pv}} = V_{pv} - V_{dc} \tag{41}$$

The corresponding current slopes are

$$\frac{di_s}{dt} = \frac{v_s - V_{dc}}{L_f} \tag{42}$$

$$\frac{di_{pv}}{dt} = \frac{V_{pv} - V_{dc}}{L_{pv}} \tag{43}$$

Since the PV boost converter operates in boost mode, normally Vdc>Vpv, so the PV inductor current decreases while delivering power to the DC link.

Applying the volt-second balance principle to the grid-side inductor over one switching period gives

$$d_1(v_s) + (1 - d_1)(v_s - V_{dc}) = 0 \tag{44}$$

which simplifies to

$$V_{dc} = \frac{v_s}{1 - d_1} \tag{45}$$

where d1 is the duty ratio associated with the PFC switching action. Similarly, for the PV boost inductor, volt-second balance gives

$$d_{pv}(V_{pv}) + (1 - d_{pv})(V_{pv} - V_{dc}) = 0 \tag{46}$$

which yields

$$V_{dc} = \frac{V_{pv}}{1 - d_{pv}} \tag{47}$$

where dpv is the duty ratio of the PV boost switch Spv.

The average grid current is controlled to follow the grid voltage reference for power factor correction. Therefore,

$$i_s^* = \frac{2P^*}{V_m} \sin \omega t \tag{48}$$

where is∗ is the reference grid current, P∗ is the reference input power, Vm is the peak grid voltage, and ω is the angular frequency. This ensures that the input current remains sinusoidal and in phase with the supply voltage, resulting in near-unity power factor.

The PV output power is given by

$$P_{pv} = V_{pv} I_{pv} \tag{49}$$

and this power is transferred to the DC link through the boost converter. The total power at the DC link can be expressed as

$$P_{dc} = P_{grid} + P_{pv} \tag{50}$$

ignoring converter losses. This combined power supports the EV-side load and maintains the DC-link voltage constant. During the negative half cycle, the operation is similar, except that S3 remains ON and S4 remains OFF. The switching behavior of S1, S2, and Spv follows the same principle. Thus, the converter achieves symmetrical

operation in both half cycles while maintaining PFC action and PV power injection. Overall, the totem-pole PFC converter shapes the grid current and regulates the DC-link voltage, whereas the PV boost converter extracts solar power and feeds it into the same DC link. The coordinated switching of S1, S2, S3, S4, and Spv enables simultaneous grid interfacing, PV power transfer, and efficient supply to the EV charging stage.

VII. Controller designing of Totem Pole Converter

The control of the single-phase totem-pole converter is based on a two-loop control structure, consisting of an outer DC-link voltage control loop and an inner grid current control loop. The objective of the controller is to regulate the DC-link voltage while ensuring that the input current is sinusoidal and in phase with the grid voltage, achieving unity power factor.

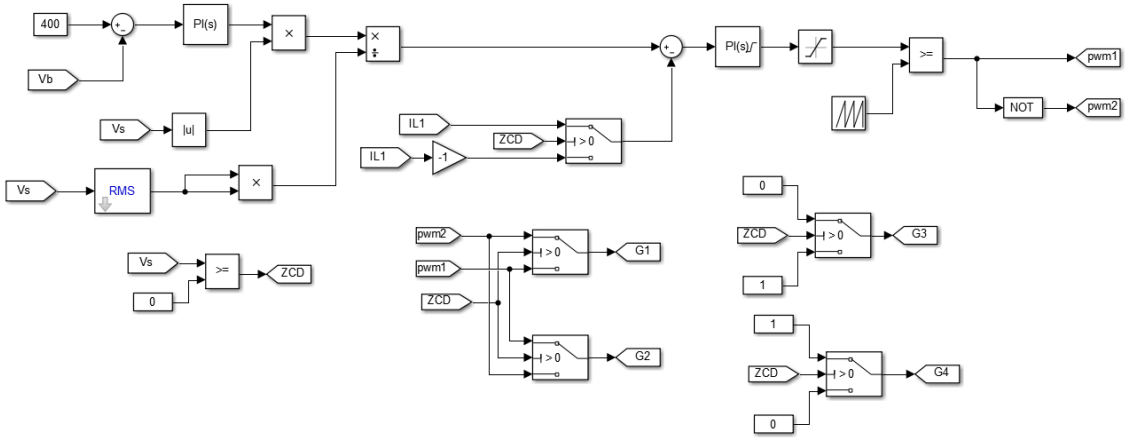

Fig. 8. Control Strategy of Single-Phase Totem-Pole PFC Converter

A. Outer Voltage Control Loop

The DC-link voltage is regulated by comparing the reference voltage Vdcref with the measured DC-link voltage Vdc. The error is given by

$$e_v = V_{dc}^{ref} - V_{dc} \tag{51}$$

This error is processed through a PI controller to generate the reference current magnitude:

$$I_{ref} = K_p e_v + K_i \int e_v \, dt \tag{52}$$

This output represents the amplitude of the reference grid current required to maintain the DC-link voltage.

B. Reference Current Generation

The instantaneous grid voltage vs is normalized using its RMS value to generate a unit sinusoidal signal:

$$u_s = \frac{v_s}{V_{s,rms}} \tag{53}$$

The reference current is then obtained as

$$i_s^* = I_{ref} \cdot u_s \tag{54}$$

This ensures that the reference current follows the grid voltage waveform, achieving unity power factor operation.

C. Inner Current Control Loop

The actual grid current is is compared with the reference current is∗, and the error is given by

$$e_i = i_s^* - i_s \tag{55}$$

This signal represents the required voltage across the inductor to shape the current.

D. PWM Generation

The control signal is compared with a high-frequency carrier waveform to generate PWM pulses:

$$\text{PWM} = \begin{cases} 1, & v_{control} > v_{carrier} \\ 0, & \text{otherwise} \end{cases} \tag{56}$$

The generated PWM signals are used to control switches S1 and S2.

E. Switching Logic

The operation of switches S3 and S4 depends on the polarity of the grid voltage:

- For positive half cycle (vs>0):

$$S_4 = ON, \quad S_3 = OFF \tag{57}$$

- For negative half cycle (vs<0):

$$S_3 = ON, \quad S_4 = OFF \tag{58}$$

The complementary switching of S1 and S2 is given by:

$$S_2 = \overline{S_1} \tag{59}$$

F. Inductor Current Dynamics

The grid-side inductor voltage is given by

$$v_L = L\frac{di_s}{dt} \tag{60}$$

During switching:

- When switch is ON:

$$v_L = L\frac{di_s}{dt} \tag{61}$$

During switching:

- When switch is ON:

$$v_L = v_s \tag{62}$$

- When switch is OFF:

$$v_L = v_s - V_{dc} \tag{63}$$

VIII. SIMULATION RESULTS AND DISCUSSION

A. Performance Analysis of the Proposed Bidirectional EV Onboard Charger

The simulation results validate the performance of the proposed bidirectional EV onboard charger based on the interleaved totem-pole front-end converter and bidirectional push–pull converter under different operating conditions. From the grid-side waveforms, the grid voltage remains sinusoidal throughout the simulation with a peak magnitude of nearly 230 V to 250 V, confirming a stable single-phase input supply. The grid current shows dynamic variation according to the charging and discharging conditions of the EV battery. During the initial interval from 0 to 0.2 s, the grid current oscillates with a comparatively high magnitude, reaching about 60 A to 70 A, which indicates active power transfer from the grid to the dc-link and battery. From 0.2 s to 0.4 s, the current magnitude reduces to nearly20 A to ±30 A, showing a lower power demand. Around 0.4 s to 0.6 s, the current becomes very small, close to 0 A, indicating a light-load or transition region. After 0.6 s, the current rises again and varies within approximately 20 A to ±40 A, confirming renewed power exchange with the battery. The near-sinusoidal current profile shows that the front-end converter maintains good power quality and proper current shaping. The PV voltage and PV current plots show the contribution of the solar source to the dc-link. Initially, the PV voltage remains around 245–250 V from 0 to 0.4 s, while the PV current is about 20 A from 0 to 0.2 s and then decreases to nearly 10 A between 0.2 s and 0.4 s. At t ≈ 0.4 s, the PV current drops to almost 0 A, and the PV voltage also reduces from nearly 250 V to around 130 V, then gradually settles near 110–120 V by the end of the simulation. This behavior indicates a change in solar operating condition or irradiance level, causing the PV source to contribute less power after 0.4 s. Accordingly, the dc-link is then supported mainly by the grid and the EV battery depending on the operating mode. The dc-link voltage Vdc remains regulated around its reference despite source and load variations, which confirms the effectiveness of the control strategy. At the starting instant, the dc-link voltage rises rapidly and briefly reaches about 470–480 V, then settles within the range of 390–410 V. Between 0.1 s and 0.8 s, the dc-link voltage remains close to 400 V with only limited ripple. A slight disturbance is observed near 0.8 s, where the dc-link voltage rises again to nearly 440–450 V, after which it returns and settles around 400–410 V. This shows that the proposed control maintains good dc-bus regulation even during power transitions. The EV-side waveforms clearly show the bidirectional charging and discharging operation. The EV battery voltage Vev remains almost constant around 104 V over most of the simulation, which indicates stable battery terminal voltage. A small increase is observed between 0.6 s and 0.8 s, where the battery voltage rises to approximately 104.6–104.8 V, followed by a slight drop after 0.8 s, settling near 103.8–104 V. The EV current Iev confirms the operating modes more clearly. From 0 to 0.6 s, the EV current remains close to 0 A, indicating either standby or very low charging current. At t ≈ 0.6 s, the current becomes negative and drops to

nearly −25 A, and then further to about −35 A at t ≈ 0.7 s, indicating grid-to-vehicle charging mode, where energy is transferred into the EV battery. At t ≈ 0.8 s, the current reverses direction and becomes positive, reaching nearly 20 A, and then increases to about 35 A after 0.9 s, indicating vehicle-to-grid operation, where the battery starts delivering power back to the system. This current reversal clearly verifies the bidirectional capability of the proposed onboard charger. The EV state of charge (SOC) plot also supports this behavior. The SOC remains nearly constant at about 84.490% from 0 to 0.6 s, then increases slightly and reaches about 84.4915% near 0.8 s, corresponding to the charging interval. After 0.8 s, the SOC begins to decrease gradually and returns toward 84.490% by 1 s, which is consistent with the discharging or V2G interval. Although the SOC variation is small due to the short simulation time, the trend confirms correct battery energy flow in both directions. Overall, the simulation results demonstrate that the proposed onboard charger achieves stable and efficient operation under dynamic conditions. The totem-pole front-end maintains a nearly sinusoidal input current and good dc-link voltage regulation, while the bidirectional push–pull stage enables controlled charging and discharging of the EV battery. The PV source supports the dc-link during the initial interval, and the system successfully transitions between different modes without instability. Therefore, the proposed topology offers improved power quality, reliable bidirectional energy transfer, and effective integration of grid, PV, and EV battery systems for advanced G2V and V2G applications.

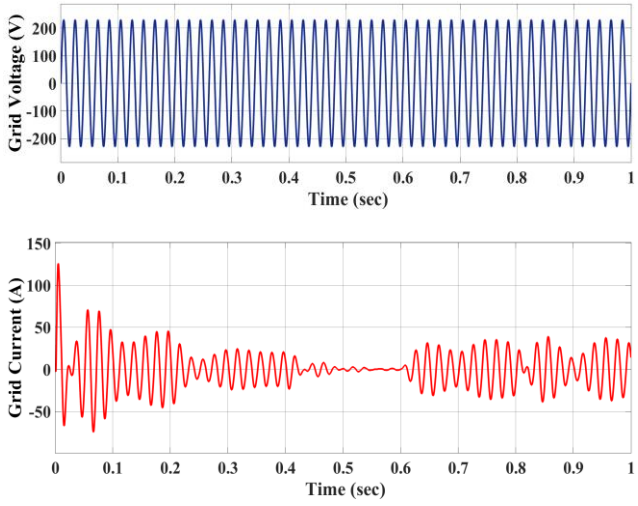

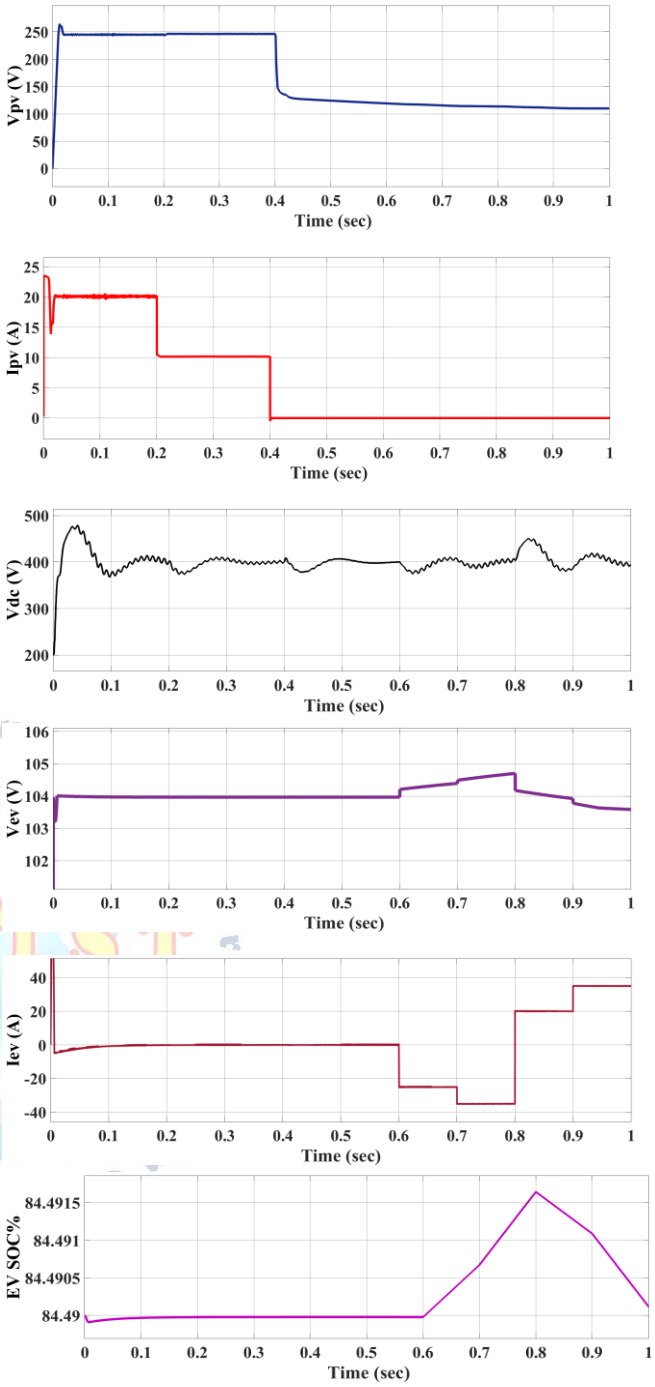

Fig.9 Simulation Results and Performance Analysis of the Proposed Bidirectional EV Onboard Charger

B. Power Factor Correction Performance of Totem-Pole Converter

The performance of the totem-pole converter in terms of power quality is validated through the power factor analysis. As observed in the waveform, the input current closely follows the grid voltage, indicating proper synchronization and effective current shaping. The calculated power factor is maintained at approximately 0.985, which is very close to unity. This confirms that the proposed totem-pole converter successfully achieves

near-unity power factor correction, thereby reducing reactive power consumption and improving overall system efficiency.

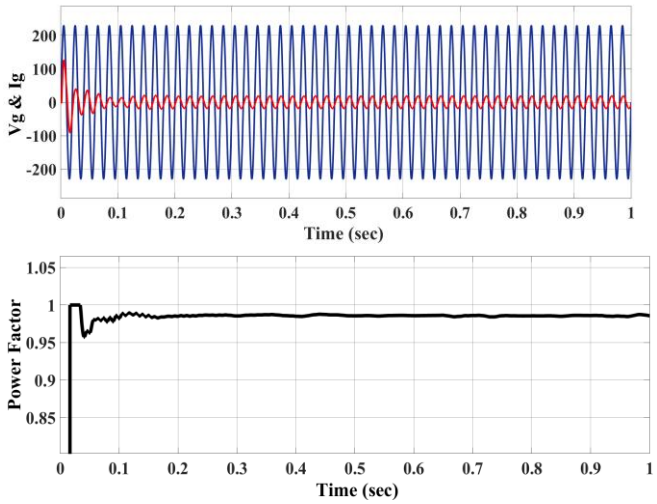

Fig.10 Simulation results of Power Factor Correction Performance of Totem-Pole Converter

C. Dynamic Power Variation and Energy Management under PV and EV Operating Conditions

The dynamic power variation of the proposed grid–PV–EV system under different solar and EV load conditions is presented in terms of kW. The results clearly show coordinated power sharing among the grid, PV system, and EV battery over the time interval 0 to 1 s. At the initial instant, a transient is observed where the grid power briefly reaches about 10 kW, after which it quickly stabilizes. The PV power settles around 4.5 kW to 5 kW, while the EV power remains close to 0 kW, indicating that the EV is not actively participating in power exchange during the startup period. From 0 to 0.2 s, the PV system supplies approximately 5 kW, acting as the primary source. During this interval, the grid power becomes negative, varying between −8 kW and −3 kW, indicating power flow from the system toward the grid or reduced grid consumption depending on the sign convention. The EV remains inactive with power close to 0 kW. Between 0.2 s and 0.4 s, the PV power reduces to around 2.5 kW, indicating a drop in solar generation. Consequently, the grid compensates for this reduction, with its power varying between approximately −5 kW and −2 kW. The EV still remains in idle mode during this interval. From 0.4 s to 0.6 s, the PV power further decreases to nearly 0 kW, indicating minimal or no solar contribution. During this period, the grid power approaches 0 kW, showing a balanced or low-demand condition, while the EV power remains negligible. At $t \approx 0.6$ s, the EV starts participating in the system. The EV power becomes negative, reaching about −2.5 kW to −3.5 kW, which indicates charging mode (grid-to-vehicle). During this time, the grid power becomes slightly positive (around 0 to 1 kW), supplying the required energy for battery charging. Between 0.6 s and 0.8 s, the EV continues charging, and its power varies within −3 kW to −4 kW, while the grid supplies the necessary power to maintain system balance. The PV contribution remains minimal in this interval. At $t \approx 0.8$ s, the EV power reverses direction and becomes positive, rising to approximately 2 kW to 3.5 kW, indicating vehicle-to-grid (V2G) operation, where the EV battery supplies power back to the system. Correspondingly, the grid power becomes negative again, varying roughly between −3 kW and −5 kW, showing reduced dependence on the grid. From 0.8 s to 1 s, the EV continues discharging, and the system maintains balanced power flow among sources. The PV power remains close to zero, and the grid adjusts dynamically to maintain equilibrium. Overall, the results demonstrate that the proposed system effectively manages dynamic power sharing in kW, enabling smooth transitions between PV generation, grid support, and EV charging/discharging modes. The system successfully achieves coordinated operation under varying solar and EV load conditions, confirming its suitability for bidirectional V2G applications with efficient power management.

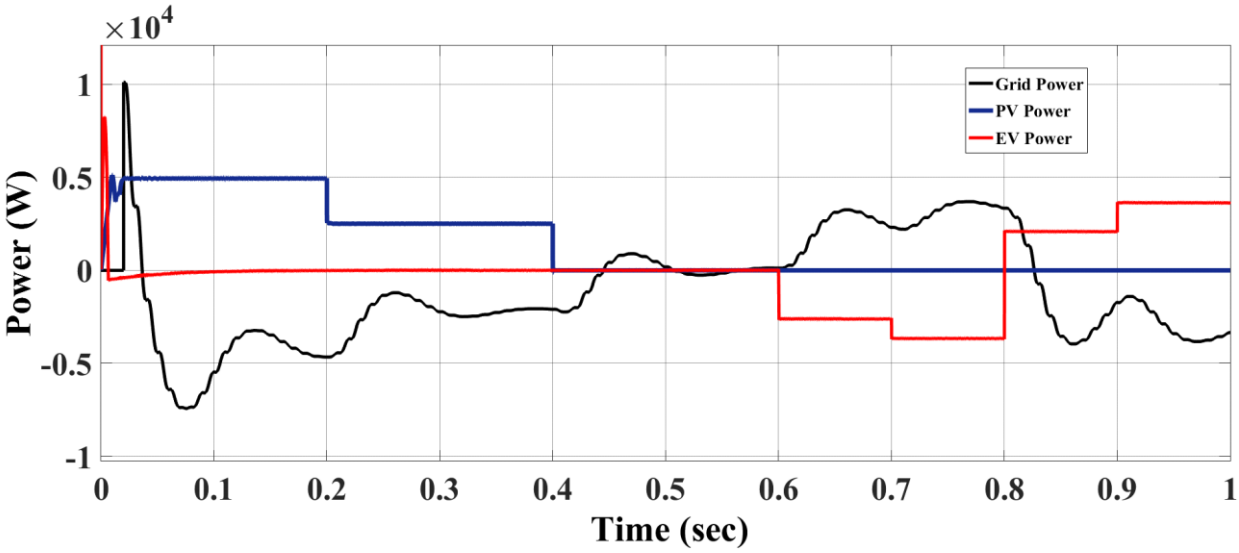

Fig.11 Simulation results of Dynamic Power Variation and Energy Management under PV and EV Operating Conditions

IX. CONCLUSION

This paper presented a power-quality-optimized bidirectional EV onboard charger based on an interleaved totem-pole AC–DC converter integrated with a bidirectional push–pull DC–DC stage for V2G applications. The proposed topology successfully eliminates the conventional diode bridge rectifier and reduces the number of power conversion stages, thereby minimizing conduction losses and improving overall efficiency and power density. The simulation results demonstrate that the totem-pole front-end converter achieves near-unity power factor (approximately 0.985) with low input current distortion, ensuring high power quality at the grid interface. The interleaved structure effectively reduces current ripple and improves thermal performance, contributing to reliable and efficient operation. The DC-link voltage is well regulated under varying operating conditions, confirming the effectiveness of the implemented control strategy. The bidirectional capability of the proposed system is validated through seamless transitions between grid-to-vehicle (G2V) and vehicle-to-grid (V2G) modes. The EV battery is charged and discharged in a controlled manner under constant current and constant voltage conditions, while maintaining stable voltage and current profiles. Additionally, the dynamic power variation results confirm proper coordination between grid, PV (if integrated), and EV, ensuring balanced power flow under different load and generation scenarios. Overall, the proposed onboard charger offers a reliable, efficient, and flexible solution for next-generation EV charging systems. It significantly enhances power quality, reduces losses, and enables effective bidirectional energy transfer, making it well suited for smart grid and grid-interactive EV applications. Future work may focus on hardware implementation and advanced control optimization to further improve system performance and scalability.

Conflict of interest statement

Authors declare that they do not have any conflict of interest.

REFERENCES

[1] S. S. G. Acharige, Md. E. Haque, M. T. Arif, N. Hosseinzadeh, K. N. Hasan, and A. M. T. Oo, ''Reviewof electric vehicle charging technologies, standards, architectures, and converter configurations,'' IEEE Access, vol. 11, pp. 41218–41255, 2023, doi: 10.1109/ACCESS.2023.3267164.

[2] A. Khaligh and M. D'Antonio, ''Global trends in high-power on-board chargers for electric vehicles,'' IEEE Trans. Veh. Technol., vol. 68, no. 4, pp. 3306–3324, Apr. 2019, doi: 10.1109/TVT.2019.2897050.

[3] R. Pradhan, N. Keshmiri, and A. Emadi, ''On-board chargers for highvoltage electric vehicle powertrains: Future trends and challenges,'' IEEE Open J. Power Electron., vol. 4, pp. 189–207, 2023, doi: 10.1109/OJPEL.2023.3251992.

[4] H. Nazi, E. Babaei, S. Tohidi, and M. Liserre, ''An isolated SRC-based single phase single stage battery charger for electric vehicles,'' IEEE Trans. Transport. Electrific., vol. 9, no. 1, pp. 1252–1262, Mar. 2023, doi: 10.1109/TTE.2022.3185018.

[5] D. Zinchenko, A. Blinov, A. Chub, D. Vinnikov, I. Verbytskyi, and S. Bayhan, ''High-efficiency single-stage on-board charger for electrical vehicles,'' IEEE Trans. Veh. Technol., vol. 70, no. 12, pp. 12581–12592, Dec. 2021, doi: 10.1109/TVT.2021.3118392.

[6] S.-G. Jeong, Y.-S. Jeong, J.-M. Kwon, and B.-H. Kwon, ''A soft-switching single-stage converter with high efficiency for a 3.3-kW on-board charger,'' IEEE Trans. Ind. Electron., vol. 66, no. 9, pp. 6959–6967, Sep. 2019, doi: 10.1109/TIE.2018.2877093.

[7] S. S. Sayed and A. M. Massoud, ''Review on state-of-the-art unidirectional non-isolated power factor correction converters for short-/long-distance electric vehicles,'' IEEE Access, vol. 10, pp. 11308–11340, 2022, doi: 10.1109/ACCESS.2022.3146410.

[8] R. Pandey and B. Singh, ''Canonical switching cell (CSC) converterbased power factor-corrected battery charger for e-rickshaw,'' IEEE Trans. Ind. Appl., vol. 56, no. 5, pp. 5046–5055, Sep. 2020, doi: 10.1109/TIA.2020.2996539.

[9] R. Kushwaha, V. Khadkikar, and A. Edpuganti, ''Electric vehicle onboard fast charging through converter maximum switch utilization,'' IEEE Trans. Power Electron., vol. 39, no. 1, pp. 998–1014, Jan. 2024, doi: 10.1109/TPEL.2023.3321760. 121566

[10] G. K. Naveen Kumar, A. K. Verma, and N. Sandeep, ''Improved gain single-phase buck-boost PFC with wide output voltage range for universal input EV applications,'' IEEE Trans. Ind. Electron., vol. 72, no. 1, pp. 299–307, Jan. 2025.

[11] R. Patil and S. P. Prakash, ''Performance enhancement of switchedcapacitor- based bridgeless buck PFC rectifier,'' IEEE Trans. Power Electron., vol. 39, no. 3, pp. 2938–2942, Mar. 2024, doi: 10.1109/TPEL.2023.3340701.

[12] G. Li, D. Yang, B. Zhou, Y.-F. Liu, and H. Zhang, ''A topology reconfigurable fault-tolerant two-and-single stage AC–DC converter for high reliability applications,'' IEEE Trans. Ind. Electron., vol. 70, no. 4, pp. 3708–3716, Apr. 2023, doi: 10.1109/TIE.2022.3174236.

[13] S. R. Meher and R. K. Singh, ''A standard two stage on-board charger with single controlled PWM and minimum switch count,'' IEEE Trans. Ind. Appl., vol. 59, no. 4, pp. 4628–4639, Jul. 2023, doi: 10.1109/TIA.2023.3267334.

[14] J. Lu, A. Mallik, S. Zou, and A. Khaligh, ''Variable DC-link control loop design for an integrated two-stage AC/DC converter,'' IEEE Trans. Transport. Electrific., vol. 4, no. 1, pp. 99–107, Mar. 2018, doi: 10.1109/TTE.2017.2755772.

[15] P. Dadhaniya, M. Maurya, and G. M. Vishwanath, ''A bridgeless modified boost converter to improve power factor in EV battery charging applications,'' IEEE J. Emerg. Sel. Topics Ind. Electron., vol. 5, no. 2, pp. 553–564, Apr. 2024, doi: 10.1109/JESTIE.2024.3355887.

[16] L. Xue, Z. Shen, D. Boroyevich, P. Mattavelli, and D. Diaz, ''Dual active bridge-based battery charger for plug-in hybrid electric vehicle with charging current containing low frequency ripple,'' IEEE Trans. Power Electron., vol. 30, no. 12, pp. 7299–7307, Dec. 2015, doi: 10.1109/TPEL.2015.2413815.

[17] S. A. Assadi, H. Matsumoto, M. Moshirvaziri, M. Nasr, M. S. Zaman, and O. Trescases, ''Active saturation mitigation in high-density dual-activebridge DC–DC converter for on-board EV charger applications,'' IEEE Trans. Power Electron., vol. 35, no. 4, pp. 4376–4387, Apr. 2020, doi: 10.1109/TPEL.2019.2939301.

[18] V. R. K. Kanamarlapudi, B.Wang, N. K. Kandasamy, and P. L. So, ''A new ZVS full-bridge DC–DC converter for battery charging with reduced losses over full-load range,'' IEEE Trans. Ind. Appl., vol. 54, no. 1, pp. 571–579, Jan. 2018, doi: 10.1109/TIA.2017.2756031.

[19] N. Hou, Y. Zhang, and Y. W. Li, ''A natural transient-behavior-based control theory for DAB-based two-stage DC–DC converter,'' IEEE Trans. Power Electron., vol. 38, no. 12, pp. 15137–15141, Dec. 2023, doi: 10.1109/TPEL.2023.3316642.

[20] S. Harinaik, S. Sathyan, and N. J. M. Mary, ''Design and analysis of modified series–parallel quasiresonant half-bridge DC/DC converter for renewable energy applications,'' IEEE J. Emerg. Sel. Topics Ind. Electron., vol. 5, no. 3, pp. 1089–1099, Jul. 2024.